Letter

Superconductivity in doped triangular Mott insulators: The roles of parent spin backgrounds and charge kinetic energy

Zheng Zhu [1,2,*] and Qianqian Chen [1,†]

[1] *Kavli Institute for Theoretical Sciences, University of Chinese Academy of Sciences, Beijing 100190, China*

[2] *CAS Center for Excellence in Topological Quantum Computation, University of Chinese Academy of Sciences, Beijing 100190, China*

(Received 4 October 2022; revised 18 May 2023; accepted 19 May 2023; published 6 June 2023)

We study the prerequisites for realizing superconductivity in doped triangular-lattice Mott insulators by considering three distinct parent spin backgrounds, i.e., 120° antiferromagnets, quantum spin liquid, and stripy antiferromagnets, and all possible sign combinations (τ_1, τ_2) of nearest-neighbor hopping and next-nearest-neighbor hopping (t_1, t_2). Based on density matrix renormalization group calculations, we find that, with finite t_2 and specific sign combinations (τ_1, τ_2), the quasi-long-range superconductivity order can always be achieved, regardless of the nature of the parent spin backgrounds. Besides specific hopping signs (τ_1, τ_2), these superconductivity phases in triangular lattices are commonly characterized by short-ranged spin correlations and two charges per stripe. In the robust superconductivity phase realized at larger t_2/t_1, flipping the signs τ_2 and τ_1 gives rise to the stripe phase without strong pairing and a pseudogaplike phase without Cooper-pair phase coherence, respectively. Interestingly, the roles of the two hopping signs are switched at smaller t_2/t_1. Moreover, different sign combinations (τ_1, τ_2) would stabilize distinct phases including superconductivity, charge density waves, spin density waves, and pseudogaplike phases accordingly. Our findings suggest the important role of charge kinetic energy in realizing superconductivity in doped triangular-lattice Mott insulators.

DOI: 10.1103/PhysRevB.107.L220502

Introduction. Understanding the superconductivity (SC) that emerges from doping Mott insulators has been a long-standing issue in physics. Unlike the conventional Bardeen-Cooper-Schrieffer (BCS) superconductivity [1], the prerequisites for achieving superconductivity in doped Mott insulators remain elusive [2–17]. The general understanding originates from doping quantum spin liquids (QSLs) [18–22], which is composed of condensed spin resonating-valence-bond pairs such that doped charges have an energetic incentive to pair [2,6,9]. The superconductivity arises when those pairs achieve long-range phase coherence. However, besides QSL, the parent spin backgrounds usually host various magnetic orders, then it is highly instructive to explore the doped distinct magnetic ordered Mott insulators to fully reveal the prerequisites for realizing superconductivity. Moreover, since the interplay between the doped charge and the spin backgrounds determines the charge properties [4–6,12,14], it is also fundamentally significant to identify the role of charge kinetic energy in the resulting superconductivity.

Tremendous efforts on this issue have been devoted to the square lattice [2–17] since the discovery of high-temperature superconductivity in cuprates. Nevertheless, such studies on the triangular lattice have equal importance and the geometric frustrations bring even richer physics for both Mott insulators [23–31] and doped Mott insulators [32–53], as revealed in earlier experimental discoveries of superconductivity in $Na_xCoO_2 \cdot yH_2O$ [54,55]. Remarkably, distinct hopping signs are inequivalent on a triangular lattice [41,48]. More recently, both the cold-atom and condensed-matter experiments have offered additional platforms to probe the doped triangular-lattice Mott insulators with a wide range of parameters in a well-controlled manner, such as loading ultracold fermions onto a triangular optical lattice [56,57], stacking two distinct transition-metal dichalcogenides (TMDs) such as WSe_2/WS_2 heterobilayers [58–61], depositing atomic layers on semiconductor substrates such as Sn/Si(111) [62], and doping organic compounds [63,64]. Remarkably, these platforms host different parent spin backgrounds and different sign combinations in charge hoppings [54,55,58–64], laying the experimental foundations for studying the roles of Mott insulation and kinetic energy in the resulting superconductivity.

Motivated by the above, we examine the roles of the parent spin backgrounds and the charge hopping signs in achieving triangular-lattice superconductivity. We consider three distinct spin backgrounds realized in the J_1-J_2 model,

$$H_{J_1\text{-}J_2} = J_1 \sum_{\langle ij\rangle} \mathbf{S}_i \cdot \mathbf{S}_j + J_2 \sum_{\langle\langle ij\rangle\rangle} \mathbf{S}_i \cdot \mathbf{S}_j, \tag{1}$$

where $\langle ij\rangle$ and $\langle\langle ij\rangle\rangle$ denote the nearest-neighbor (NN) and next-nearest-neighbor (NNN) bonds, respectively. The undoped spin backgrounds are 120° antiferromagnetic (AFM) at $J_2/J_1 \lesssim 0.07 \sim 0.08$, stripy AFM at $J_2/J_1 \gtrsim 0.15$–0.16, and QSL in between [65–76], as shown in Fig. 1(b). The motion of the doped charge can be captured by

$$H_{t_1-t_2} = \tau_1|t_1|\mathcal{P}\sum_{\langle ij\rangle\sigma}(c_{i\sigma}^{\dagger}c_{j\sigma} + \text{H.c.})\mathcal{P} + \tau_2|t_2|\mathcal{P}\sum_{\langle\langle ij\rangle\rangle\sigma}(c_{i\sigma}^{\dagger}c_{j\sigma} + \text{H.c.})\mathcal{P}, \tag{2}$$

*zhuzheng@ucas.ac.cn

†chenqianqian@ucas.ac.cn

(a)

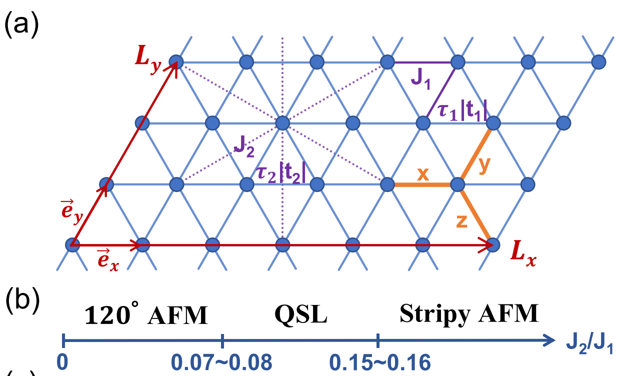

(c)

(τ_1,τ_2) \ J_2/J_1	0.03 (120°AFM)	0.05 (120° AFM)	0.12 (QSL)	0.24 (Stripy AFM)
(+, +)	Stripe ($n_s \approx 1$)	Stripe ($n_s = 1$)	Stripe ($n_s = 1$)	SDW / Stripe ($n_s = 1$)
(−, +)	Stripe / SC ($n_s = 2$ bulk)	Stripe ($n_s \approx 1$)	Stripe ($n_s \approx 1$)	Stripe ($n_s = 1$)
(−, −)	Stripe ($n_s = 2$) / PG-like	SC ($n_s = 2$)	SC ($n_s = 2$)	SC ($n_s = 2$)
(+, −)	Stripe ($n_s \approx 1$)	Stripe ($n_s = 2$) / PG-like	Stripe ($n_s = 2$) / PG-like	PG-like / Stripe ($n_s = 2$)

FIG. 1. (a) Sketch of triangular lattice and model parameters. (b) Phase diagram of J_1-J_2 Heisenberg model. (c) The most dominant correlations in lightly doped Mott insulators on YC4 cylinders controlled by $J_2/J_1 = (t_2/t_1)^2$ for different hopping signs (τ_1, τ_2).

where $c_{i\sigma}^\dagger$ is the fermion creation operator, and $\mathcal{P}$ projects to the single-occupancy subspace. $\tau_1 = \pm$ ($\tau_2 = \pm$) denote the signs of NN hopping t_1 (NNN hopping t_2). The different sign combinations (τ_1, τ_2) are physically reasonable because they correspond to different materials [54,55,58–64]. Physically, $J_2/J_1 = (t_2/t_1)^2$ since (2) is an effective Hamiltonian of the Hubbard model in the strong-coupling limit.

We study the ground-state properties by density matrix renormalization group (DMRG) [77,78]. To examine the roles of Mott insulation after doping, we focus on light doping and study three distinct Mott insulators by tuning J_2/J_1. The triangular lattice is spanned by the primitive vectors $\mathbf{e_x}$, $\mathbf{e_y}$ and wrapped on YC cylinders [see Fig. 1(a)]. The system size is $N = L_x \times L_y$, where L_x (L_y) represents the cylinder length (circumference). The doping concentration is $\delta = N_0/N$, with N_0 denoting the number of doped charges, which could represent either electrons or holes, depending on the fermion charge. Here, we mainly study $L_y = 4, 6$ and also examine $L_y = 5, 8$. Due to the different rates of convergence at different parameters, the bond dimension is pushed up to $D = 40\,000$ when implementing $U(1) \times U(1)$ symmetry and $D = 16\,000$ when implementing $SU(2) \times U(1)$ symmetry.

Main findings. By studying the lightly doped three distinct Mott insulators (i.e., 120° AFM, QSL, and stripy AFM) with all possible hopping signs (τ_1, τ_2), we conclude our findings in Fig. 1(c). First, the quasi-long-range superconductivity order can be realized regardless of the nature of the undoped parent Mott insulators, provided specific hopping signs. Second, the quasi-long-range superconductivity ordered phase in a triangular lattice is commonly featured by the short-ranged spin correlations and two-charge filled stripes per one-dimensional unit cell in the bulk. Third, at larger J_2/J_1, sign τ_1 determines the Cooper-pair phase coherence for the superconductivity phase, whereas sign τ_2 is relevant to the charge pairing for all phases. Flipping the signs τ_1 and τ_2 from the robust superconductivity phase would give rise to pseudogaplike behavior and charge stripes without strong pairing, respectively. Interestingly, their roles interchange at smaller J_2/J_1. Fourth, specific sign combinations (τ_1, τ_2) would stabilize distinct phases at larger J_2/J_1 including SC, charge density wave (CDW), spin density wave (SDW), and pseudogap (PG)-like phase.

Unlike previous studies of the same model which only focus on $(\tau_1, \tau_2) = (-, -)$ in QSL [42,43] or the 120° AFM [43] parent spin background to search for superconductivity, in this Letter, we consider three distinct parent spin backgrounds, i.e., 120° AFM, QSL, and stripy AFM, and all possible signs $(\tau_1, \tau_2) = (\pm, \pm)$ to understand how to achieve superconductivity, as well as revealing different correlated phases stabilized by specific sign combinations such as SC, CDW, SDW, and PG-like phases. Moreover, we focus on very light doping in order to examine the role of Mott insulation, thus our focused doping concentration and J_2/J_1 are also different. Considering the DMRG cylinders break the rotational symmetry, the identification of pairing symmetry is not our focus [79].

Pair correlations for distinct (τ_1, τ_2). We begin by examining the pair correlations

$$D_{\alpha\beta}(\mathbf{r}) \equiv \langle \hat{\Delta}_\alpha^\dagger(\mathbf{r_0}) \hat{\Delta}_\beta(\mathbf{r_0} + \mathbf{r}) \rangle, \tag{3}$$

where the pair operator is $\hat{\Delta}_\alpha(\mathbf{r}) \equiv \frac{1}{\sqrt{2}} \sum_\sigma \sigma c_{\mathbf{r},\sigma} c_{\mathbf{r}+\mathbf{e}_\alpha,-\sigma}$ and $\alpha, \beta = x, y, z$. In quasi-one-dimensional cylinders, the true long-range superconductivity order is forbidden based on the Mermin-Wagner theorem, so we look for quasi-long-range order $D_{\alpha\beta}(\mathbf{r}) \sim r^{-\eta_{sc}}$. In particular, $\eta_{sc} < 2$ suggests divergent SC susceptibility in two dimensions (2D).

We compute the pair correlations for all (τ_1, τ_2) in lightly doped spin backgrounds: 120° AFM [Figs. 2(a) and 2(c)], QSL [Fig. 2(e)], and stripy AFM [Fig. 2(g)]. We choose typical parameters of each parent phase and find that the power-law-decayed pair correlations can always be realized at certain signs (τ_1, τ_2). As shown in Figs. 2(a) and 2(c), although the parent spin backgrounds are the same, the power-law-decayed pair correlations emerge at $(\tau_1, \tau_2) = (-, +)$ with $1 < \eta_{sc} < 2$ when $J_2/J_1 = 0.03, 0.01$ for $L_y = 4$ while they switch to $(\tau_1, \tau_2) = (-, -)$ with a much slower decay rate $\eta_{sc} \approx 0.82$ for $J_2/J_1 = 0.05$. Further increasing the ratio J_2/J_1 deep inside the parent spin background QSL with $J_2/J_1 = 0.12$ or the stripy AFM with $J_2/J_1 = 0.24$ [see Figs. 2(e) and 2(g)], the pair correlations at $(\tau_1, \tau_2) = (-, -)$ become fairly strong against distance with exponent $\eta_{sc} \lesssim 1$, suggesting the robust superconductivity in both cases. Moreover, the main features are qualitatively consistent when increasing the doping or the system size, as Figs. 2(b), 2(d) 2(f), and 2(h) show, and the pair correlations become weakened with increasing doping. On wider cylinders with widths larger than $L_y = 4$, as shown in Fig. 4(a), we also find algebraically decayed pair correlations at light doping with $\eta_{sc} \approx 1.6$ for $L_y = 5$, $\eta_{sc} \approx 1.4$ for $L_y = 6$, and $\eta_{sc} \approx 1.3$ for $L_y = 8$. The exponent $\eta_{sc} < 2$ suggests robust SC with

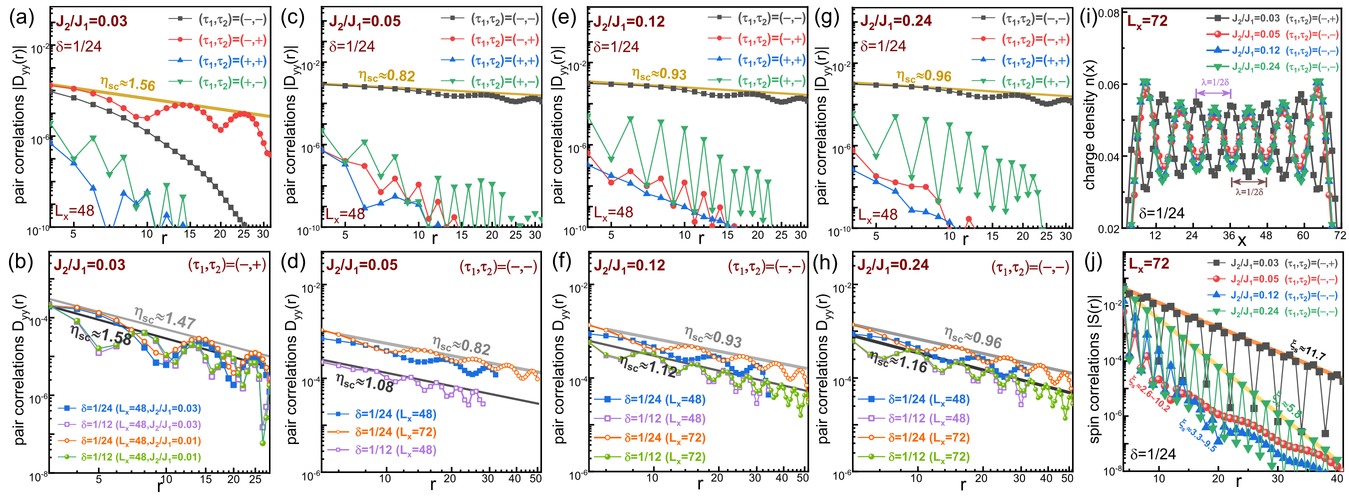

FIG. 2. (a)–(h) The pair correlations for all hopping signs $(\tau_1, \tau_2) = (\pm, \pm)$ in lightly doped three parent Mott insulating spin backgrounds: (a)–(d) 120° AFM, (e), (f) QSL, and (g), (h) stripy AFM. Here, we consider systems with $L_y = 4$ and $\delta = 1/24, 1/12$. (i), (j) The charge density distribution (i) and the spin correlations (j) at the parameters with quasi-long-range superconductivity order.

divergent susceptibility towards 2D. These results illustrate that superconductivity can be obtained from doping distinct Mott insulators, not only from the QSL. More crucially, the realization of superconductivity requires specific hopping signs and finite NNN hopping.

The common features for phases with quasi-long-range superconductivity order. Although the parent spin backgrounds are distinct before doping, there are common features when the quasi-long-range SC order establishes after doping.

In the charge sector, we examine the charge density distribution, which is uniform along $\mathbf{e_y}$ on cylinders, so we focus on the distribution along $\mathbf{e_x}$ and define $n(x) \equiv 1/L_y \sum_y \langle 1 - \hat{n}_e(x, y)\rangle$. As shown in Fig. 2(i) for $L_y = 4$ and Fig. 4(b) for $L_y = 5, 6, 8$, the charge profiles exhibit stripe patterns with specific charge numbers in each stripe. For specific (τ_1, τ_2) with quasi-long-range SC order, there are two doped charges per unit cell if we view the cylinders as one-dimensional systems, i.e., $n_s = 2$ with n_s denoting the number of doped charges in each stripe on average, consistent with the existence of strong pairing.

In the spin sector, we compute the spin correlations $S(r) \equiv \langle \mathbf{S}(\mathbf{r_0}) \cdot \mathbf{S}(\mathbf{r_0} + r\mathbf{e_x})\rangle$. For specific (τ_1, τ_2) with quasi-long-range SC order, the spins commonly exhibit short-ranged correlations with finite decay length ξ_s, as shown in Fig. 2(j) for $L_y = 4$ and Fig. 4(c) for wider cylinders with $L_y = 5, 6, 8$. In particular, we find the increased decay length on wider cylinders; however, it tends to saturate when further increasing cylinder length (width) for a fixed width (length) [79], e.g., unchanged ξ_s when increasing L_x for fixed $L_y = 6$ [see Fig. 4(c)]. We remark that, although the parent spin background could be distinct before doping, when the SC emerges after doping, the spin correlations become short ranged.

The effect of hopping signs (τ_1, τ_2) on robust superconductivity at larger J_2/J_1. To identify the roles of hopping signs in superconductivity, we start from a robust superconductivity phase and examine the effect of flipping the signs τ_1, τ_2. The robust superconductivity is characterized by power-law-decayed pair correlations and the dominant pair correlations over other correlations, which occur at $J_2/J_1 \gtrsim 0.05$ when $(\tau_1, \tau_2) = (-, -)$ [see Figs. 2(c), 2(e), 2(g), and 3(a)]. To compare various correlations at light doping δ, we define the renormalized correlations, including (i) the single-particle propagator $\mathrm{CC}(r) \equiv [C(r)/\delta]^2$ where $C(r) = \sum_\sigma \langle c^\dagger_\sigma(\mathbf{r_0}) c_\sigma(\mathbf{r_0} + r\mathbf{e_x})\rangle$, (ii) the spin correlations $\mathrm{SS}(r) \equiv |S(r)|$, (iii) the pair correlations $\mathrm{DD}(r) \equiv |D_{yy}(r)|/\delta^2$, and (iv) the charge density correlations $\mathrm{NN}(r) \equiv |N(r)|/\delta^2$, where $N(r) = \langle n(\mathbf{r_0}) n(\mathbf{r_0} + r\mathbf{e_x})\rangle - \langle n(\mathbf{r_0})\rangle \langle n(\mathbf{r_0} + r\mathbf{e_x})\rangle$.

As shown in Fig. 3(a) for $(\tau_1, \tau_2) = (-, -)$, the pair correlations with exponent $\eta_{\mathrm{sc}} \approx 0.96$ dominate over other correlations. We remark that here $\eta_{\mathrm{sc}} < 1 < \eta_{\mathrm{cdw}}$ is consistent

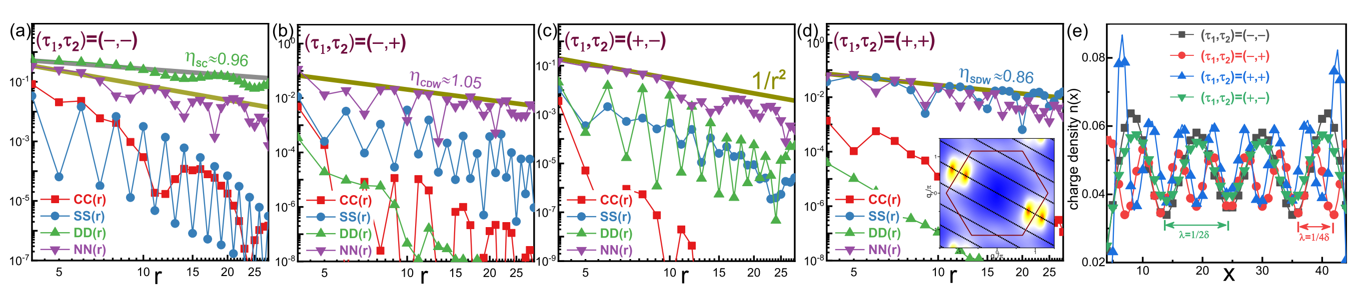

FIG. 3. Various correlations for distinct hopping signs $(\tau_1, \tau_2) = (\pm, \pm)$ (a)–(d) at a lightly doped ($\delta = 1/24$) stripy AFM parent spin background. (e) The charge density distributions for distinct (τ_1, τ_2). Here, we consider $J_2/J_1 = 0.24$ (stripy AFM) on $N = 48 \times 4$ cylinders. The doped QSL with $J_2/J_1 = 0.12$ and doped 120° AFM with $J_2/J_1 = 0.05$ exhibit similar behavior [79].

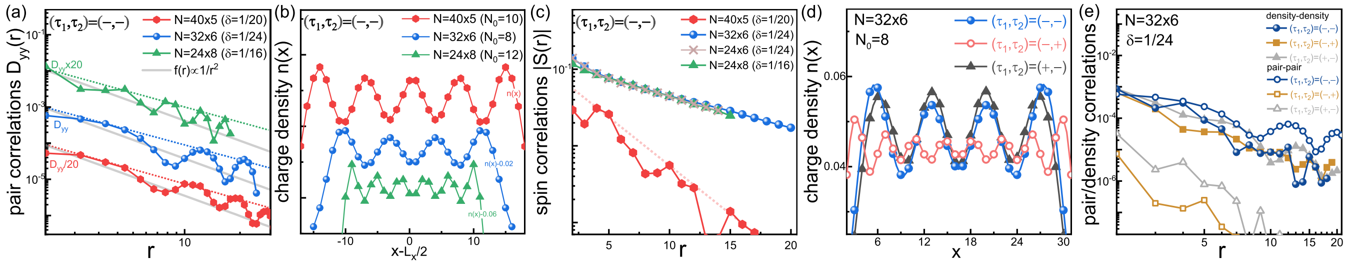

FIG. 4. (a) The pair correlations, (b) charge density distribution, and (c) spin correlations on wider cylinders with $L_y = 5, 6, 8$ for $J_2/J_1 = 0.24$. Starting from $(\tau_1, \tau_2) = (-, -)$ with quasi-long-range SC order, (d) and (e) show the effect of flipping the hopping sign τ_2 and τ_1.

with the Luther-Emery liquid behavior [80]. By only switching τ_2, as shown in Fig. 3(b), the charge density correlations become dominant instead, while the pair correlations are significantly suppressed. Meanwhile, the change of n_s from 2 to 1 [see Fig. 3(e)] implies the breaking of Cooper pairs. This suggests the sign of NNN hopping is relevant to the charge pairing. By contrast, when only switching τ_1, we also find the suppressed pair correlations but with strong fluctuations [see Fig. 3(c)], and all other correlations decay faster than r^{-2}. Since both signs of τ_1 exhibit $n_s = 2$ stripes [see Fig. 3(e)], the charge pairs are robust, consistent with a pseudogap behavior, where the doped charges form pairs but the phase coherence is lacking. This suggests the sign of NN hopping is relevant to the phase coherence among pairs. When simultaneously switching both signs, as shown in Fig. 3(d), the spin correlations are remarkably enhanced and decay slightly slower than the charge density correlations, demonstrating the robust SDWs. The spin structure factor [see the inset of Fig. 3(d)] suggests an incommensurate SDW. We remark that the above results are obtained for doped stripy AFM at $J_2/J_1 = 0.24$, the doped QSL, and doped 120° AFM at $J_2/J_1 = 0.05$ exhibit similar behavior [79].

Moreover, we further confirm the roles of τ_2 and τ_1 on wider cylinders. As shown in Fig. 4(d) for $L_y = 6$ cylinders, when starting from $(\tau_1, \tau_2) = (-, -)$ with quasi-long-range SC order, flipping the sign τ_2 would change n_s from 2 to 1, consistent with breaking Cooper pairs. By contrast, flipping τ_1 does not break Cooper pairs. However, either flipping the sign τ_2 or τ_1 would significantly suppress the pair correlations, as shown in Fig. 4(e), while the charge density correlations remain robust. These observations suggest the hopping signs are relevant to charge pairing and phase coherence.

The effect of hopping signs (τ_1, τ_2) *on pair correlations at smaller* J_2/J_1. At smaller J_2/J_1, we find algebraically decayed pair correlations when $(\tau_1, \tau_2) = (-, +)$ with $1 < \eta_{sc} < 2$ on $L_y = 4$ cylinders [see Figs. 2(a) and 2(b)]. Notably, the pair correlations decay at a comparable rate with the charge density correlations, exhibiting competing quasi-long-range orders. Since $\eta_{cdw} \lesssim \eta_{sc}$, the stripe order is slightly dominant. The existence of competing orders is also reflected in the convergence of DMRG, which becomes much harder than larger J_2/J_1. With the increase of system size, it also requires a larger bond dimension to ensure the convergence of correlations at a longer distance [see Fig. 5(b)]. We notice that the charge profiles exhibit a two-charge filled stripe pattern only in the bulk, while the boundaries host separate single charge [see Figs. 2(i) and 5(d)].

Compared with other sign combinations, $(\tau_1, \tau_2) = (-, +)$ indeed enhances the pair correlations at smaller J_2/J_1 [see Fig. 2(a)]. Now we start from $(\tau_1, \tau_2) = (-, +)$ to examine the effect of switching the signs τ_1, τ_2. We will show the interchanged roles of τ_1, τ_2 at smaller J_2/J_1 compared with the larger J_2/J_1. After solely switching τ_2, as Fig. 5(b) shows, the pair correlations are strongly suppressed. Meanwhile, the single-particle propagator and spin fluctuations are also significantly suppressed. Given the robust two-charge filled stripe pattern shown in Fig. 5(d), the resulting phase hosts the robust local pairing. The absence of quasi-long-range order is induced by the lack of phase coherence among pairs. Here, we remark that the pair correlations in this parameter regime also exhibit strong anisotropy [79]. These observations are consistent with a pseudogaplike behavior, and the role of sign τ_2 at smaller J_2/J_1 is similar to the role of sign τ_1 at larger J_2/J_1 [see Fig. 3(c)]. Furthermore, if only switching τ_1, as shown in Fig. 5(c), the pair correlations are dramatically suppressed, while the charge profile also implies the loosened strong pairing [see Fig. 5(d)]. These findings suggest that τ_1 may play a role in the formation of strongly paired charges, similar to the effect of τ_2 at higher J_2/J_1[see Fig. 3(b)]. When simultaneously switching both signs (τ_1, τ_2), the charge density correlations become the most dominant ones [79].

Summary and discussion. In summary, we study how to realize superconductivity in lightly doped triangular-lattice Mott insulators in the strong-coupling limit. By considering three distinct undoped parent spin backgrounds and all possible sign combinations of the NN and NNN hoppings, we find that, provided with finite NNN hopping and specific sign combinations, superconductivity can always be realized with doping distinct Mott insulators, not only the QSL. The superconductivity phase is commonly featured by short-ranged spin correlations and two charges per stripe. Moreover, switching the sign τ_2 (τ_1) in a robust superconductivity phase would result in the stripe phase without strong pairing (pseudogaplike phase without Cooper-pair phase coherence) at larger J_2/J_1, whereas their roles interchange at smaller J_2/J_1. We also reveal that different sign combinations stabilize distinct correlated phases, including SC, CDW, SDW, and PG-like phases. Our findings suggest the importance of kinetic energy in realizing superconductivity, which may stimulate future studies on the superconductivity mechanism and on examining different sign combinations for other lattice geometries and their intrinsic connections to a previously studied square-lattice case [12,14,81,82]. Considering different triangular-lattice materials correspond to different

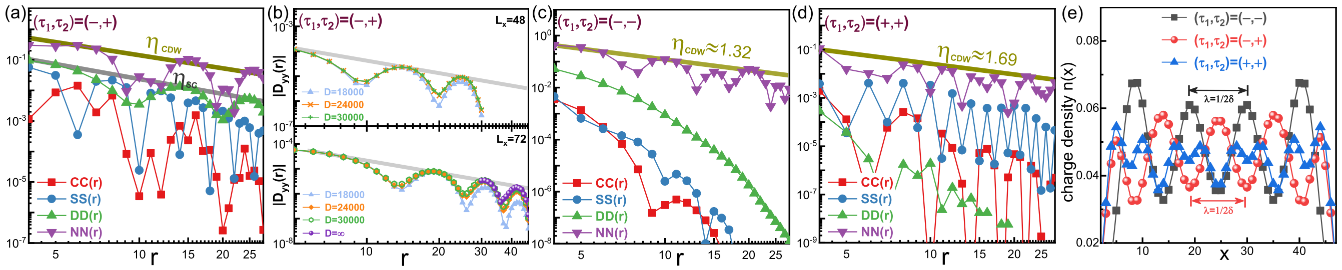

FIG. 5. (a), (c), (d) Various correlations for distinct hopping signs (τ_1, τ_2) at smaller J_2/J_1. Here, we consider $J_2/J_1 = 0.03$ at $\delta = 1/24$ on $N = 48 \times 4$ cylinders. (b) shows the convergence of pair correlations for different lattice sizes and (e) shows the charge density distributions. Other parameters $J_2/J_1 = 0.02, 0.01$ exhibit similar behavior [79].

sign combinations in hopping terms [54,55,58–64,83,84], our findings of distinct correlated phases stabilized by specific hopping sign combinations can be potentially probed.

Z.Z. is particularly grateful to A. Vishwanath, D. N. Sheng, and S. A. Chen for previous collaborations on the triangular-lattice Hubbard model and helpful discussions on this work. We also particularly thank insightful discussions with Z.-Y. Weng. This work was supported by the National Natural Science Foundation of China (Grant No. 12074375), the Fundamental Research Funds for the Central Universities, the Strategic Priority Research Program of CAS (Grant No. XDB33000000), and Innovation Program for Quantum Science and Technology (Grant No. 2-6).

[1] J. Bardeen, L. N. Cooper, and J. R. Schrieffer, Theory of superconductivity, Phys. Rev. **108**, 1175 (1957).
[2] P. W. Anderson, The resonating valence bond state in La_2CuO_4 and superconductivity, Science **235**, 1196 (1987).
[3] F. C. Zhang and T. M. Rice, Effective Hamiltonian for the superconducting Cu oxides, Phys. Rev. B **37**, 3759 (1988).
[4] E. Dagotto, Correlated electrons in high-temperature superconductors, Rev. Mod. Phys. **66**, 763 (1994).
[5] D. N. Sheng, Y. C. Chen, and Z. Y. Weng, Phase String Effect in a Doped Antiferromagnet, Phys. Rev. Lett. **77**, 5102 (1996).
[6] P. A. Lee, N. Nagaosa, and X.-G. Wen, Doping a Mott insulator: Physics of high-temperature superconductivity, Rev. Mod. Phys. **78**, 17 (2006).
[7] X.-G. Wen and P. A. Lee, Theory of Underdoped Cuprates, Phys. Rev. Lett. **76**, 503 (1996).
[8] L. Balents and S. Sachdev, Dual vortex theory of doped Mott insulators, Ann. Phys. **322**, 2635 (2007).
[9] B. Keimer, S. A. Kivelson, M. R. Norman, S. Uchida, and J. Zaanen, From quantum matter to high-temperature superconductivity in copper oxides, Nature (London) **518**, 179 (2015).
[10] E. Fradkin, S. A. Kivelson, and J. M. Tranquada, Colloquium: Theory of intertwined orders in high temperature superconductors, Rev. Mod. Phys. **87**, 457 (2015).
[11] T. Senthil and P. A. Lee, Cuprates as doped $U(1)$ spin liquids, Phys. Rev. B **71**, 174515 (2005).
[12] K. Wu, Z. Y. Weng, and J. Zaanen, Sign structure of the t-J model, Phys. Rev. B **77**, 155102 (2008).
[13] Z.-Y. Weng, Superconducting ground state of a doped Mott insulator, New J. Phys. **13**, 103039 (2011).
[14] Z. Zhu, H. C. Jiang, D. N. Sheng, and Z. Y. Weng, Nature of strong hole pairing in doped Mott antiferromagnets, Sci. Rep. **4**, 5419 (2014).
[15] Z. Zhu, D. N. Sheng, and Z.-Y. Weng, Pairing versus phase coherence of doped holes in distinct quantum spin backgrounds, Phys. Rev. B **97**, 115144 (2018).
[16] D. P. Arovas, E. Berg, S. A. Kivelson, and S. Raghu, The Hubbard model, Annu. Rev. Condens. Matter Phys. **13**, 239 (2022).
[17] M. Qin, T. Schäfer, S. Andergassen, P. Corboz, and E. Gull, The Hubbard model: A computational perspective, Annu. Rev. Condens. Matter Phys. **13**, 275 (2022).
[18] L. Balents, Spin liquids in frustrated magnets, Nature (London) **464**, 199 (2010).
[19] L. Savary and L. Balents, Quantum spin liquids: a review, Rep. Prog. Phys. **80**, 016502 (2017).
[20] Y. Zhou, K. Kanoda, and T.-K. Ng, Quantum spin liquid states, Rev. Mod. Phys. **89**, 025003 (2017).
[21] C. Broholm, R. J. Cava, S. A. Kivelson, D. G. Nocera, M. R. Norman, and T. Senthil, Quantum spin liquids, Science **367**, eaay0668 (2020).
[22] J. Knolle and R. Moessner, A field guide to spin liquids, Annu. Rev. Condens. Matter Phys. **10**, 451 (2019).
[23] H. Saarikoski, J. E. Vázquez-Lozano, J. P. Baltanás, F. Nagasawa, J. Nitta, and D. Frustaglia, Topological transitions in spin interferometers, Phys. Rev. B **91**, 241406(R) (2015).
[24] T. Shirakawa, T. Tohyama, J. Kokalj, S. Sota, and S. Yunoki, Ground-state phase diagram of the triangular lattice Hubbard model by the density-matrix renormalization group method, Phys. Rev. B **96**, 205130 (2017).
[25] A. Szasz, J. Motruk, M. P. Zaletel, and J. E. Moore, Chiral Spin Liquid Phase of the Triangular Lattice Hubbard Model: A Density Matrix Renormalization Group Study, Phys. Rev. X **10**, 021042 (2020).
[26] Y.-H. Zhang, D. N. Sheng, and A. Vishwanath, SU(4) Chiral Spin Liquid, Exciton Supersolid, and Electric Detection in Moiré Bilayers, Phys. Rev. Lett. **127**, 247701 (2021).
[27] B.-B. Chen, Z. Chen, S.-S. Gong, D. N. Sheng, W. Li, and A. Weichselbaum, Quantum spin liquid with emergent chiral order in the triangular-lattice Hubbard model, Phys. Rev. B **106**, 094420 (2022).

[28] A. Wietek, R. Rossi, F. Šimkovic, M. Klett, P. Hansmann, M. Ferrero, E. M. Stoudenmire, T. Schäfer, and A. Georges, Mott Insulating States with Competing Orders in the Triangular Lattice Hubbard Model, Phys. Rev. X **11**, 041013 (2021).

[29] T. Cookmeyer, J. Motruk, and J. E. Moore, Four-Spin Terms and the Origin of the Chiral Spin Liquid in Mott Insulators on the Triangular Lattice, Phys. Rev. Lett. **127**, 087201 (2021).

[30] A. Szasz and J. Motruk, Phase diagram of the anisotropic triangular lattice Hubbard model, Phys. Rev. B **103**, 235132 (2021).

[31] Y. Zhou, D. N. Sheng, and E.-A. Kim, Quantum Phases of Transition Metal Dichalcogenide Moiré Systems, Phys. Rev. Lett. **128**, 157602 (2022).

[32] G. Baskaran, Electronic Model for CoO_2 Layer Based Systems: Chiral Resonating Valence Bond Metal and Superconductivity, Phys. Rev. Lett. **91**, 097003 (2003).

[33] T. Watanabe, H. Yokoyama, Y. Tanaka, J.-i. Inoue, and M. Ogata, Variational Monte Carlo studies of pairing symmetry for the t-J model on a triangular lattice, J. Phys. Soc. Jpn. **73**, 3404 (2004).

[34] O. I. Motrunich and P. A. Lee, Possible effects of charge frustration in Na_xCoO_2: Bandwidth suppression, charge orders, and resurrected resonating valence bond superconductivity, Phys. Rev. B **69**, 214516 (2004).

[35] O. I. Motrunich and P. A. Lee, Study of the triangular lattice tV model near $x = \frac{1}{3}$, Phys. Rev. B **70**, 024514 (2004).

[36] Q.-H. Wang, D.-H. Lee, and P. A. Lee, Doped t-J model on a triangular lattice: Possible application to $Na_xCoO_2 \cdot yH_2O$ and $Na_{1-x}TiO_2$, Phys. Rev. B **69**, 092504 (2004).

[37] B. Kumar and B. S. Shastry, Superconductivity in CoO_2 layers and the resonating valence bond mean-field theory of the triangular lattice t-J model, Phys. Rev. B **68**, 104508 (2003).

[38] S. Zhou and Z. Wang, Nodal $d + id$ Pairing and Topological Phases on the Triangular Lattice of $Na_xCoO_2 \cdot yH_2O$: Evidence for an Unconventional Superconducting State, Phys. Rev. Lett. **100**, 217002 (2008).

[39] S. Raghu, S. A. Kivelson, and D. J. Scalapino, Superconductivity in the repulsive Hubbard model: An asymptotically exact weak-coupling solution, Phys. Rev. B **81**, 224505 (2010).

[40] M. L. Kiesel, C. Platt, W. Hanke, and R. Thomale, Model Evidence of an Anisotropic Chiral $d+id$-Wave Pairing State for the Water-Intercalated $Na_xCoO_2 \cdot yH_2O$ Superconductor, Phys. Rev. Lett. **111**, 097001 (2013).

[41] Z. Zhu, D. N. Sheng, and A. Vishwanath, Doped Mott insulators in the triangular-lattice Hubbard model, Phys. Rev. B **105**, 205110 (2022).

[42] H. C. Jiang, Superconductivity in the doped quantum spin liquid on the triangular lattice, npj Quantum Mater. **6**, 71 (2021).

[43] Y. Huang, S.-S. Gong, and D. N. Sheng, Quantum Phase Diagram and Spontaneously Emergent Topological Chiral Superconductivity in Doped Triangular-Lattice Mott Insulators, Phys. Rev. Lett. **130**, 136003 (2023).

[44] W.-Y. He, X. Y. Xu, G. Chen, K. T. Law, and P. A. Lee, Spinon Fermi Surface in a Cluster Mott Insulator Model on a Triangular Lattice and Possible Application to $1T$-TaS_2, Phys. Rev. Lett. **121**, 046401 (2018).

[45] X.-Y. Song, A. Vishwanath, and Y.-H. Zhang, Doping the chiral spin liquid: Topological superconductor or chiral metal, Phys. Rev. B **103**, 165138 (2021).

[46] M. Qin, Effect of hole doping on the 120 degree order in the triangular lattice Hubbard model: A Hartree–Fock revisit, J. Phys.: Condens. Matter **34**, 235603 (2022).

[47] K. S. Huang, Z. Han, S. A. Kivelson, and H. Yao, Pair-density-wave in the strong coupling limit of the Holstein-Hubbard model, npj Quantum Mater. **7**, 17 (2022).

[48] S. A. Chen, Q. Chen, and Z. Zhu, Proposal for asymmetric photoemission and tunneling spectroscopies in quantum simulators of the triangular-lattice Fermi-Hubbard model, Phys. Rev. B **106**, 085138 (2022).

[49] Y.-F. Jiang and H.-C. Jiang, Topological Superconductivity in the Doped Chiral Spin Liquid on the Triangular Lattice, Phys. Rev. Lett. **125**, 157002 (2020).

[50] Y. Huang and D. N. Sheng, Topological Chiral and Nematic Superconductivity by Doping Mott Insulators on Triangular Lattice, Phys. Rev. X **12**, 031009 (2022).

[51] Y. Zhang and L. Fu, Pseudogap metal and magnetization plateau from doping moiré Mott insulator, arXiv:2209.05430.

[52] A. Wietek, J. Wang, J. Zang, J. Cano, A. Georges, and A. Millis, Tunable stripe order and weak superconductivity in the moiré Hubbard model, Phys. Rev. Res. **4**, 043048 (2022).

[53] X.-Y. Song and Y.-H. Zhang, Deconfined criticalities and dualities between chiral spin liquid, topological superconductor and charge density wave Chern insulator, arXiv:2206.08939.

[54] K. Takada, H. Sakurai, E. Takayama-Muromachi, F. Izumi, R. A. Dilanian, and T. Sasaki, Superconductivity in two-dimensional CoO_2 layers, Nature (London) **422**, 53 (2003).

[55] R. E. Schaak, T. Klimczuk, M. L. Foo, and R. J. Cava, Superconductivity phase diagram of $Na_xCoO_2 1.3H_2O$, Nature (London) **424**, 527 (2003).

[56] J. Yang, L. Liu, J. Mongkolkiattichai, and P. Schauss, Site-resolved imaging of ultracold fermions in a triangular-lattice quantum gas microscope, PRX Quantum **2**, 020344 (2021).

[57] A. Bohrdt, L. Homeier, C. Reinmoser, E. Demler, and F. Grusdt, Exploration of doped quantum magnets with ultracold atoms, Ann. Phys. **435**, 168651 (2021).

[58] Y. Tang, L. Li, T. Li, Y. Xu, S. Liu, K. Barmak, K. Watanabe, T. Taniguchi, A. H. MacDonald, J. Shan *et al.*, Simulation of Hubbard model physics in WSe_2/WS_2 moiré superlattices, Nature (London) **579**, 353 (2020).

[59] Y. Xu, S. Liu, D. A. Rhodes, K. Watanabe, T. Taniguchi, J. Hone, V. Elser, K. F. Mak, and J. Shan, Correlated insulating states at fractional fillings of moiré superlattices, Nature (London) **587**, 214 (2020).

[60] D. M. Kennes, M. Claassen, L. Xian, A. Georges, A. J. Millis, J. Hone, C. R. Dean, D. Basov, A. N. Pasupathy, and A. Rubio, Moiré heterostructures as a condensed-matter quantum simulator, Nat. Phys. **17**, 155 (2021).

[61] F. Wu, T. Lovorn, E. Tutuc, and A. H. MacDonald, Hubbard Model Physics in Transition Metal Dichalcogenide Moiré Bands, Phys. Rev. Lett. **121**, 026402 (2018).

[62] X. Wu, F. Ming, T. S. Smith, G. Liu, F. Ye, K. Wang, S. Johnston, and H. H. Weitering, Superconductivity in a Hole-Doped Mott-Insulating Triangular Adatom Layer on a Silicon Surface, Phys. Rev. Lett. **125**, 117001 (2020).

[63] H. Oike, K. Miyagawa, H. Taniguchi, and K. Kanoda, Pressure-Induced Mott Transition in an Organic Superconductor with a Finite Doping Level, Phys. Rev. Lett. **114**, 067002 (2015).

[64] H. Oike, Y. Suzuki, H. Taniguchi, Y. Seki, K. Miyagawa, and K. Kanoda, Anomalous metallic behaviour in the doped spin liquid candidate κ-$(ET)_4Hg_{2.89}Br_8$, Nat. Commun. **8**, 756 (2017).
[65] F. Wang and A. Vishwanath, Spin-liquid states on the triangular and kagomé lattices: A projective-symmetry-group analysis of Schwinger boson states, Phys. Rev. B **74**, 174423 (2006).
[66] Z. Zhu and S. R. White, Spin liquid phase of the $S = \frac{1}{2} J_1$-J_2 Heisenberg model on the triangular lattice, Phys. Rev. B **92**, 041105(R) (2015).
[67] W.-J. Hu, S.-S. Gong, W. Zhu, and D. N. Sheng, Competing spin-liquid states in the spin-$\frac{1}{2}$ Heisenberg model on the triangular lattice, Phys. Rev. B **92**, 140403(R) (2015).
[68] S. N. Saadatmand and I. P. McCulloch, Symmetry fractionalization in the topological phase of the spin-$\frac{1}{2}J_1$-J_2 triangular Heisenberg model, Phys. Rev. B **94**, 121111(R) (2016).
[69] Y. Iqbal, W.-J. Hu, R. Thomale, D. Poilblanc, and F. Becca, Spin liquid nature in the Heisenberg J_1-J_2 triangular antiferromagnet, Phys. Rev. B **93**, 144411 (2016).
[70] A. Wietek and A. M. Läuchli, Chiral spin liquid and quantum criticality in extended $S = \frac{1}{2}$ Heisenberg models on the triangular lattice, Phys. Rev. B **95**, 035141 (2017).
[71] Z. Zhu, P. A. Maksimov, S. R. White, and A. L. Chernyshev, Topography of Spin Liquids on a Triangular Lattice, Phys. Rev. Lett. **120**, 207203 (2018).
[72] S. Hu, W. Zhu, S. Eggert, and Y.-C. He, Dirac Spin Liquid on the Spin-1/2 Triangular Heisenberg Antiferromagnet, Phys. Rev. Lett. **123**, 207203 (2019).
[73] A. V. Syromyatnikov, Dynamics of spin-$\frac{1}{2}J_1$-J_2 model on the triangular lattice, Phys. Rev. B **106**, 184415 (2022).
[74] T. Tang, B. Moritz, and T. P. Devereaux, Spectra of a gapped quantum spin liquid with a strong chiral excitation on the triangular lattice, Phys. Rev. B **106**, 064428 (2022).
[75] M. Drescher, L. Vanderstraeten, R. Moessner, and F. Pollmann, Dynamical signatures of symmetry broken and liquid phases in an $S = 1/2$ Heisenberg antiferromagnet on the triangular lattice, arXiv:2209.03344.
[76] N. E. Sherman, M. Dupont, and J. E. Moore, Spectral function of the J_1-J_2 Heisenberg model on the triangular lattice, Phys. Rev. B **107**, 165146 (2023).
[77] S. R. White, Density Matrix Formulation for Quantum Renormalization Groups, Phys. Rev. Lett. **69**, 2863 (1992); Density-matrix algorithms for quantum renormalization groups, Phys. Rev. B **48**, 10345 (1993).
[78] S. Östlund and S. Rommer, Thermodynamic Limit of Density Matrix Renormalization, Phys. Rev. Lett. **75**, 3537 (1995).
[79] See Supplemental Material at http://link.aps.org/supplemental/10.1103/PhysRevB.107.L220502 for further details.
[80] A. Luther and V. J. Emery, Backward Scattering in the One-Dimensional Electron Gas, Phys. Rev. Lett. **33**, 589 (1974).
[81] Z. Zhu, D. N. Sheng, and Z.-Y. Weng, Intrinsic translational symmetry breaking in a doped Mott insulator, Phys. Rev. B **98**, 035129 (2018).
[82] S. Chen, Z. Zhu, and Z.-Y. Weng, Two-hole ground state wavefunction: Non-BCS pairing in a t-J two-leg ladder, Phys. Rev. B **98**, 245138 (2018).
[83] C. Kuhlenkamp, W. Kadow, A. Imamoglu, and M. Knap, Tunable topological order of pseudo spins in semiconductor heterostructures, arXiv:2209.05506.
[84] S. Imajo, S. Sugiura, H. Akutsu, Y. Kohama, T. Isono, T. Terashima, K. Kindo, S. Uji, and Y. Nakazawa, Extraordinary π-electron superconductivity emerging from a quantum spin liquid, Phys. Rev. Res. **3**, 033026 (2021).